西安交通大学
XI'AN JIAOTONG UNIVERSITY

World Scientific
www.worldscientific.com

Preparation and acoustic properties of high-temperature acoustic emission sensor based on La$_3$Ga$_5$SiO$_{14}$ crystal

Jingxiang Si, Changhong Yang*, Rui Guo, Yifan Wu, Xiujuan Lin and Shifeng Huang

Shandong Provincial Key Laboratory of Preparation and Measurement of Building Materials
University of Jinan, Jinan 250022, P. R. China

*mse_yangch@ujn.edu.cn

With the rapid development of modern industries, the high-temperature piezoelectric sensors that can work in extreme environments are in great demand. In this work, langasite (La$_3$Ga$_5$SiO$_{14}$, LGS), as a high-temperature piezoelectric crystal with stable electro-elastic performance, is used as core element, and air and porous Al$_2$O$_3$ are selected as backing layers respectively to prepare two kinds of high-temperature acoustic emission (AE) sensors. The detection sensitivities at 25–500°C are analyzed by the ball falling test and Hsu–Nielsen experiment. Under the condition of 25–500°C, the received amplitude signals by both sensors are maintained above 90 dB stimulated by the ZrO$_2$ ceramic ball dropping. In the Hsu–Nielsen experiment, as the temperature rising from 25°C to 500°C, the signal amplitude of sensor with air backing layer decays from 447 mV to 365 mV, while the signal amplitude varies from 270 mV to 203 mV for the sensor with porous Al$_2$O$_3$ backing layer. Significantly, compared with the bandwidth of the air-backing sensor (37–183 kHz), the sensor with porous Al$_2$O$_3$ backing layer broadens bandwidth to 28–273 kHz. These results show that both these AE sensors have strong and stable response ability to AE signals at high-temperature of 500°C. Therefore, piezoelectric AE sensor based on LGS has great potential application in the field of high-temperature structural health monitoring.

Keywords: La$_3$Ga$_5$SiO$_{14}$; acoustic emission sensor; sensitivity; structural health monitoring.

1. Introduction

At present, acoustic emission (AE) detection technology has been widely applied to structural health monitoring (SHM) in various industry fields. Due to the damage of internal structure of the material, the distribution of internal stress will change, and the local energy at the damaged place will be released quickly, transforming the mechanical energy into sound energy and propagating in a way of elastic stress wave. This phenomenon is called AE.[1,2] AE detection technology is a non-destructive testing (NDT) based on AE sensors to acutely capture AE signals generated in the process of dynamic damage of materials.[1,3–5] It can perform real-time, online and fast detection of the internal structure in the detected object without any damage.[4,6] As a consequence, AE sensors, the core component of AE technology, play a vital role in the SHM of the equipment.[7]

High-temperature industry fields require AE technology urgently to detect structure health of equipment in machinery manufacturing, automobile factory, nuclear energy and petrochemical plants and so on. For instance, nuclear energy and fossil fuel plants need to conduct SHM of steam pipes at 350°C to 580°C.[8] Wherein, AE sensors based on piezoelectric material, as one species of representative smart sensors, are expected to be applied on SHM under high-temperature. They have some significant superiorities such as attaining

real-time monitoring, detecting early fault signals and high sensitivity.[9–11] The operating principle of them is that the elastic stress wave produced by the change of the stress distribution within detected materials will be transmitted to the surface of the detected materials, letting the piezoelectric material inside the sensor attached to the surface of the detected materials receive the stress from the sound wave. Through the positive piezoelectric effect, the mechanical signal of stress wave will be converted into the voltage signal, then, the electric signal will be processed and analyzed by the computer system. Therefore, the appropriate selection of piezoelectric materials is the key to design piezoelectric AE sensors.

In recent years, high-temperature piezoelectric AE sensors have been widely studied and attracted significant attention. Commercial PZT piezoelectric ceramics, with a large piezoelectric constant d_{33} value of 300–700 pC/N, have been broadly used in AE sensors as the core functional material. In practice, with the purpose of ensuring the stability of piezoelectric devices, the operating temperature of piezoelectric devices is limited to below 1/2 Curie temperature (T_C).[11,12] However, T_C of PZT piezoelectric ceramics is as low as 360°C, which limits the working temperature of the sensors to about 150°C. Quartz crystal, as the most common piezoelectric crystal, has the advantages of a high mechanical

*Corresponding author.

quality factor Q_m value of above 10,000, high resistivity of $10^{17}\Omega\cdot$cm at room temperature, low dielectric loss value of 0.1%, and good dynamic response characteristics. Whereas, quartz crystal will produce twin structure at a temperature of 350°C, and the α-β phase transition will occur at 573°C, which adversely affects the sensitivity of the sensors and greatly reduces the operating temperature.[13–15] For AlN, the crystal structures do not undergo phase transition from room temperature to melting point of 2000°C. While the difficulties in preparation technology limit its large-scale application in the high-temperature piezoelectric AE sensors.[16–19] LiNbO$_3$ has a high Curie temperature of 1150°C and big electromechanical coupling coefficient. However, its chemical decomposition temperature (~300°C) limits the application in high-temperature environments. Specifically, it suffers from a short lifetime at elevated temperatures: 0.1 days at 450°C.[14,20,21] YCa$_4$O(BO$_3$)$_3$ is also a common high-temperature piezoelectric crystal. Johnson *et al.*[22] designed the AE sensor based on YCa$_4$O(BO$_3$)$_3$, but the temperature stability of the sensitivity needs to be improved. Compared with the piezoelectric materials mentioned above, the langasite (La$_3$Ga$_5$SiO$_{14}$, LGS) has its own unique advantages of high-temperature piezoelectric property, such as large electromechanical coupling coefficient of 16%, and stable trigonal phase from room temperature to melting point of 1470°C.[14,23,24] In addition, LGS has low dielectric loss especially below 500°C, which is suitable for working in harsh environments.[25,26] Therefore, it has potential application prospects in high-temperature fields.

In this work, two high-temperature AE sensors have been designed by using the LGS crystal as functional part and the air or porous Al$_2$O$_3$ as backing layer, and its electroacoustic performances have been studied. Under the ambient temperature in the range 25–500°C, the amplitude signals excited by the impact of ZrO$_2$ ball received by both sensors can reach above 90 dB. For the waveform signal excited by lead breaking, the amplitude range of the sensor by air backing is 365–447 mV, and the amplitude range of the sensor by porous Al$_2$O$_3$ backing is 270–203 mV. Compared with the bandwidth of sensor by air backing (37–183 kHz), the use of porous Al$_2$O$_3$ backing broadens the bandwidth to 28–274 kHz. By selecting porous material like Al$_2$O$_3$ as the backing layer, the sensitivity is reduced, but the bandwidth is broadened.

2. Experimental Method

2.1. *Preparation of high-temperature AE sensor*

In this experiment, the X-cut LGS piezoelectric crystal with a diameter of 10 mm and thickness of 1 mm was used as the sensitive element of the sensor. As shown in Fig. 1(a), the LGS single crystal is semitransparent. Based on the measurement results in Figs. 1(b)–1(d), the LGS has (l00)-orientated trigonal phase and good temperature stability for performance, featured by small changes of the resonant frequency, the electromechanical coupling coefficient k_p, the relative dielectric constant, and the dielectric loss in the temperature range 25–500°C.

The typical AE sensor is mainly composed of piezoelectric sensitive layer, shielding layer, backing layer and matching layer, which is designed and a detailed preparation process is shown in Fig. 2(a). 316 stainless steel is used as packaging shielding shell, Al$_2$O$_3$ ceramic sheet is used as the matching layer, air and porous Al$_2$O$_3$ are selected as different backing
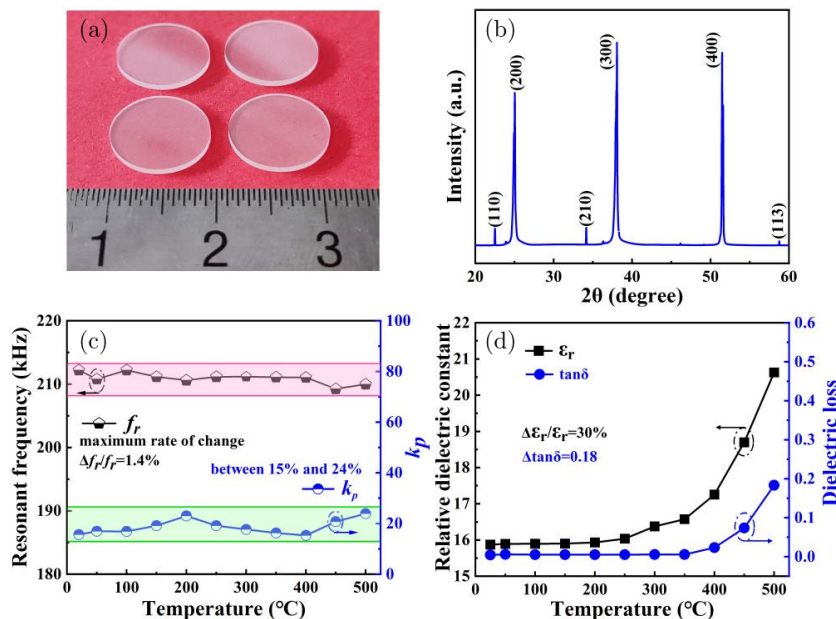

Fig. 1. (a) Physical picture of LGS single crystal, (b) a typical XRD pattern in the range 20–60°, (c) resonant frequency and electromechanical coupling coefficient under various temperatures, (d) the change of relative dielectric coefficient and dielectric loss with temperature.
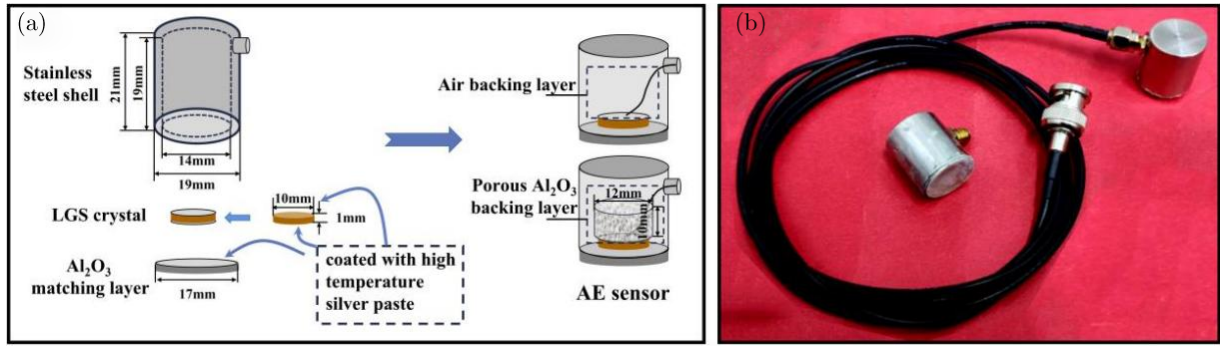
Fig. 2. The high-temperature AE sensor: (a) flow-process diagram, (b) the photographs.

layers to prepare two kinds of high-temperature AE sensors with different structures. Firstly, the Al_2O_3 ceramic sheet, and the upper and bottom surfaces of the LGS crystal were coated with high-temperature conductive silver paste, and the bottom of LGS crystal was glued to the Al_2O_3 ceramic sheet. Then the upper surface of the crystal and the core of the outer interface of the sensor were connected with a silver wire, and the bottom surface contacted the edge of the outer interface of the sensor through the stainless steel shell. Finally, the Al_2O_3 ceramic sheet and the metal shield shell were bonded together with silver adhesive. All these components must be reliably connected together to obtain good acoustic coupling. The optical images of AE sensors are shown in Fig. 2(b). In this experiment, the AE sensor based on LGS crystal with air as the backing layer is called sensor A, and the sensor with backing layer of porous Al_2O_3 is named sensor B.

As we all know, sound waves traveling through a medium will encounter resistance, i.e., acoustic impedance. Moreover, when the sound wave propagates in the medium, acoustic phenomena of reflection at the boundary of the media occur. The acoustic impedance of the backing layer is measured to evaluate the efficiency of sound energy transmission within the backing layer. The acoustic impedance can be reflected according to formula (1).[27,28] The reflection coefficient at the interface can be calculated according to formula (2)

$$Z = \rho v_c = \rho h_p / \Delta t, \tag{1}$$

$$R = \frac{Z_1 - Z}{Z + Z_1}, \tag{2}$$

where ρ, v_c, h_p, Δt, R, Z and Z_1 are the density of the backing material, sound velocity, thickness of the backing layer, time delay, reflection coefficient, acoustic impedance of backing material and measured object, respectively.

The red square wave curve is the excited signal, and the black wave is the received signal after passing through the porous Al_2O_3, as shown in Fig. 3. By calculating the difference between the time of the first peak of the received acoustic wave and that of the start of the exciting square wave, the Δt of ~13 μs can be obtained. Using this date, the acoustic impedance of porous Al_2O_3 can be calculated to be
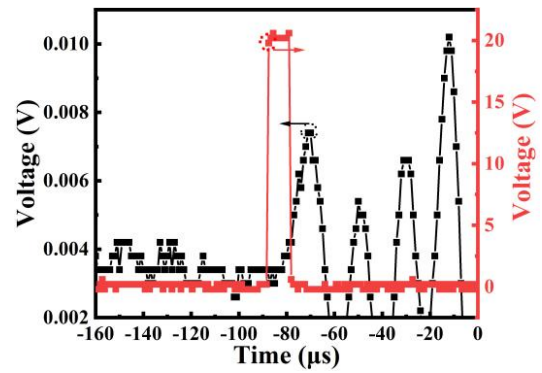

Fig. 3. The time delay test chart of porous Al_2O_3.

Table 1. Acoustic performance parameters of backing material.

Materials	ρ (kg/m³)	h_p (mm)	Δt (μs)	v_c (m/s)	Z (Mrayls)
Air	1.2	/	/	340	0.00041
Al_2O_3	895	10.004	13	769.54	0.69

0.69 Mrayls, which is much greater than the air, as listed in Table 1.

2.2. Construction of high-temperature piezoelectric AE system

In order to test the high-temperature sensing properties of AE sensors based on LGS crystal, a high-temperature AE sensor test system was built according to the principle of piezoelectric AE technology, as shown in Fig. 4. The AE sensor collects the AE signals generated by the AE source and converts them into voltage signals. Then the voltage signals are transmitted to the signal amplifier through the high-temperature armored cable. Finally, the signals are received and processed by the AEwin system. In addition, a typical AE signal is drawn in the black frame, in which the analysis parameters are defined as follows:

- Threshold: The threshold voltage level is usually set to distinguish signal from noise. AE events are counted only when the signal exceeds the threshold level.
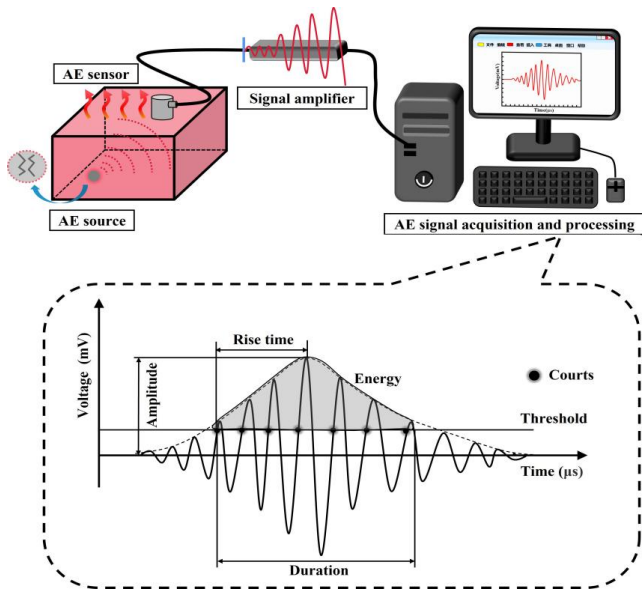
Fig. 4.   The principle of high-temperature AE technology.

- Duration: A time interval when the AE signal is just above the threshold voltage as the starting, and the signal is just below the threshold voltage as the ending.
- Counts: The number of times for the signal exceeding the threshold.
- Rise time: The interval that a signal passes above the threshold voltage to its maximum amplitude.
- Energy: the area under time versus amplitude squared curve for an event, which can be integral of the voltage value of the signal in time from the view of mathematical interpretation.

In this experiment, tubular furnace, ZrO_2 ball of diameter of 5 mm, HB pencil lead, steel ruler, high-temperature AE sensor, and Micro-II AE instrument were used to build
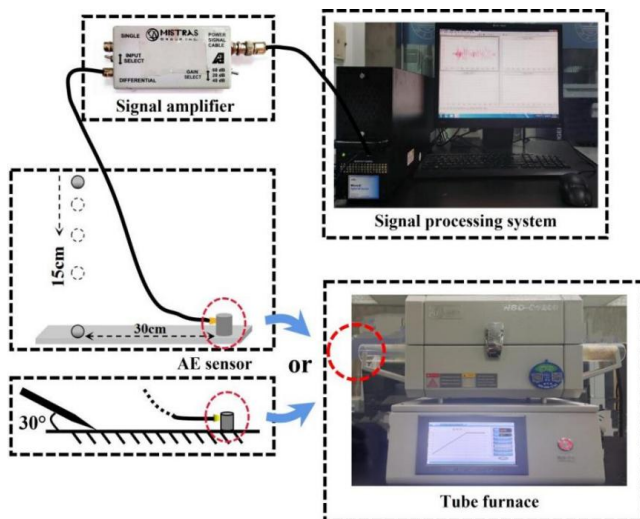

Fig. 5.   The schematic diagram of self-built AE sensor test system.

a high-temperature test system. The schematic diagram of experimental setup of the AE sensor test system is shown in Fig. 5. The steel ruler, as the test load, and the AE sensor are tightly coupled together using high-temperature inorganic adhesive. Their coupling effect has a great influence on the detection sensitivity of the sensor. The high-temperature testing environment of AE sensor is simulated by the temperature control program of tubular furnace. Specifically, the sensor is heated in a tubular furnace at a rate of 10°C/min and is set every 100°C as a test point until 500°C. The excitation signals can be generated by the free falling motion of ZrO_2 ceramic ball striking the steel ruler (H = 15 cm, S = 30 cm). Also, a pencil lead break test which was carried out according to the Hsu–Nielsen method (Φ = 0.5 mm, L = 2.5 mm, θ = 30°)[2,29] is used as the analog signals for testing the high-temperature sensing properties of the sensor. This method is an international standard experimental method, and it has been used widely in some reports such as the AE sensors based on PZT ceramics and $LiNbO_3$ crystal.[1,7]

3.   Results and Discussion

3.1.   *The ball falling tests*

The high-temperature stability of receiving acoustic signals of the AE sensor was characterized through an *in situ* high temperature ball falling test. The receiving sensitivity of AE sensors can be reflected by the amplitude of AE wave. The greater the amplitude, the higher the sensitivity of the sensor. As shown in Fig. 6, the amplitude signals of sensor A can all reach above 99 dB from room temperature to 200°C under the condition of ball collisions. As the temperature rises to 300°C continuously, the amplitude begins to fluctuate slightly. Fortunately, the average amplitude signal is 96 dB in the 10 collisions, while the maximum amplitude signal can still reach 99 dB. Even at the high-temperature of 500°C, the minimum of amplitude can be kept above 90 dB. The average amplitude attenuation from room temperature to 500°C is only about 3%. In addition, the noise thresholds from room temperature to 500°C of this high-temperature AE sensor were compared. Figure 7 shows that the noise thresholds fluctuate between 26 dB and 28 dB, and it slightly changes imperceptibly with the increase in temperature. These results indicate the suitability of sensor A for application in the temperature range 25–500°C.

For sensor B, Figs. 8(a)–8(c) illustrate the average amplitude at room temperature, which is 97 dB in the 10 collision events while it decreases only to 96 dB at 250°C. When the temperature rises to 500°C, the sensor's average amplitude is as high as 96 dB. Therefore, the amplitude signals of sensor B maintains excellent stability from room temperature to 500°C, and the amplitude signals have almost no attenuation. The noise thresholds of sensor B fluctuate from 28 dB to 32 dB in Figs. 8(a′)–8(c′), which are slightly larger than that of sensor A.
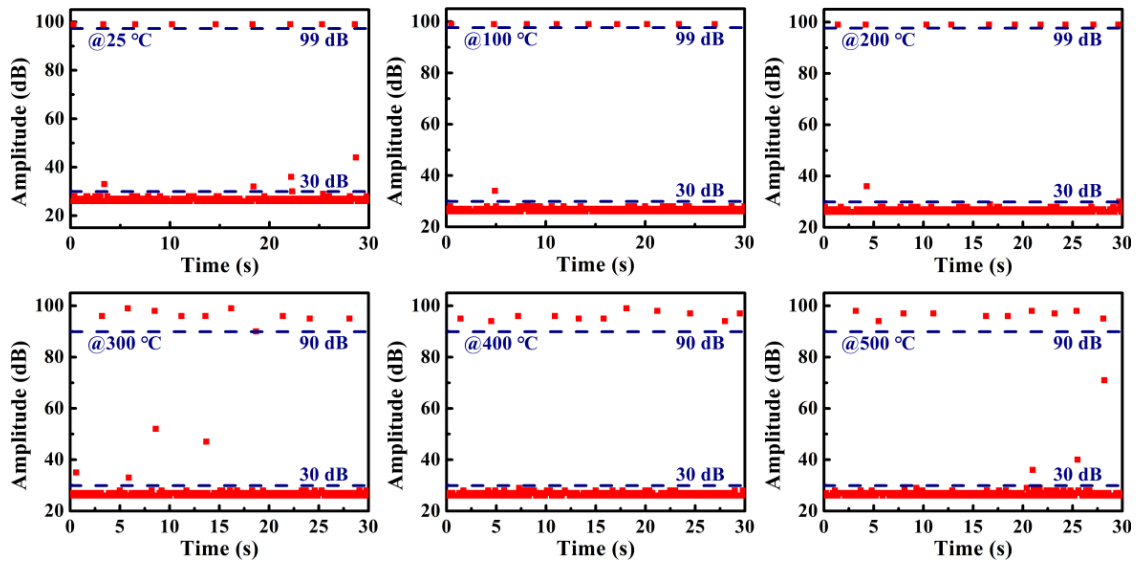
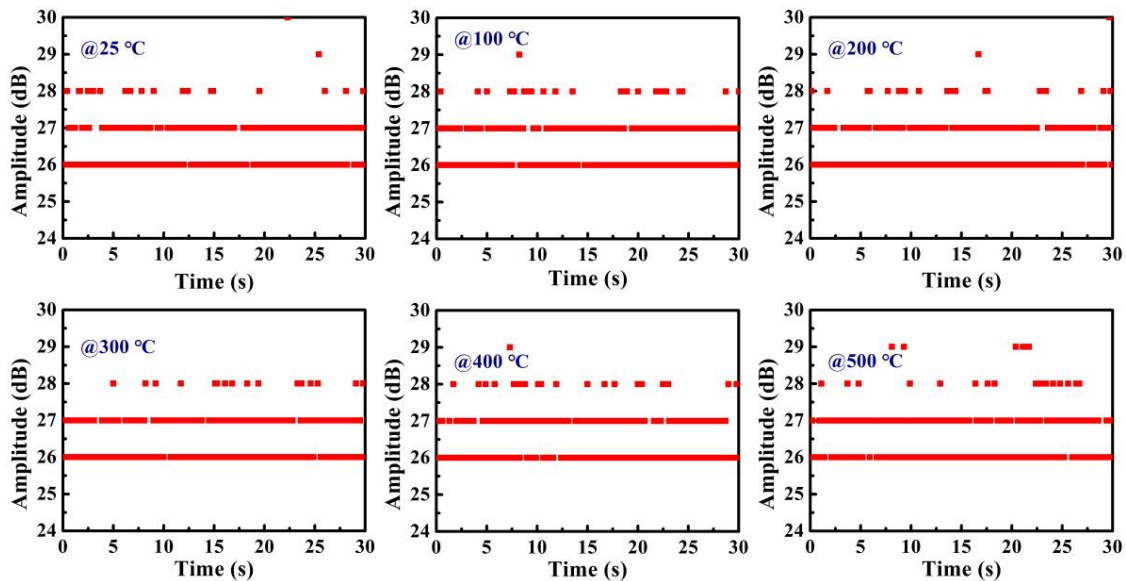Fig. 6.   Temperature-dependent amplitude signals of sensor A.

Fig. 7.   Threshold signals of sensor A under different temperatures.

3.2.   *The Hsu–Nielsen experiment*

The sensitivity of the AE sensor to the received acoustic signals was also measured and analyzed under an *in situ* high-temperature Hsu–Nielsen experiment. In each lead breaking event, the amplitude change of the lead breaking signal with time can be seen by the waveform data, then the time-domain graph can be transformed into the frequency-domain graph through the fast Fourier transform (FFT) analysis. Figure 9(a) shows the time-domain curve and the frequency–domain curve for sensor A at room temperature.

At about 21 μs after the pencil lead is broken, the AE sensor gradually receives the AE signals, and its maximum amplitude value is about 447.0 mV, which is much larger than

the AlN-based sensor of 5 mV and the LiNbO$_3$-based sensor of 34.9 mV.[7,24] Also, it can be seen that the bandwidth of sensor A is 37–183 kHz. In Fig. 9(b), for sensor B, the amplitude of maximum waveform signal is 270 mV, and the bandwidth is 28–273 kHz. Compared with sensor A, the amplitude decreases by about 40% and the bandwidth increases by about 68%.

The acoustic attenuation property is closely related with the acoustic absorption, reflection, and scatting abilities of the backing layer. According to the acoustic theory, the faster the attenuation of sound wave pulse, the smaller the amplitude of the dominant frequency, and this results in the decrease of sensitivity. Also, the acoustic attenuation is conducive to
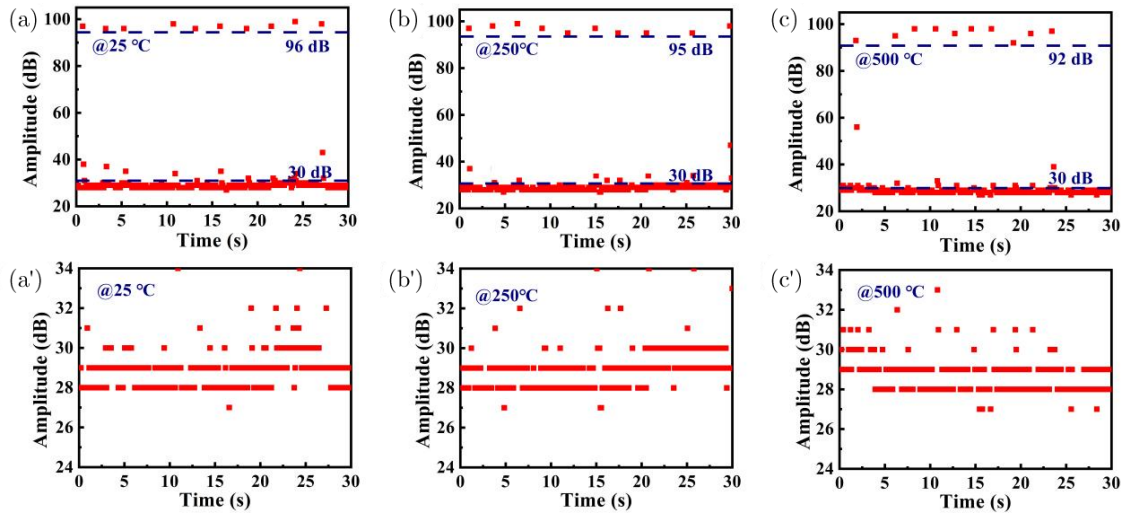
Fig. 8.   (a)–(c) Temperature dependence of amplitude signals of sensor B, (a′)–(c′) threshold signals of sensor B under different temperatures.
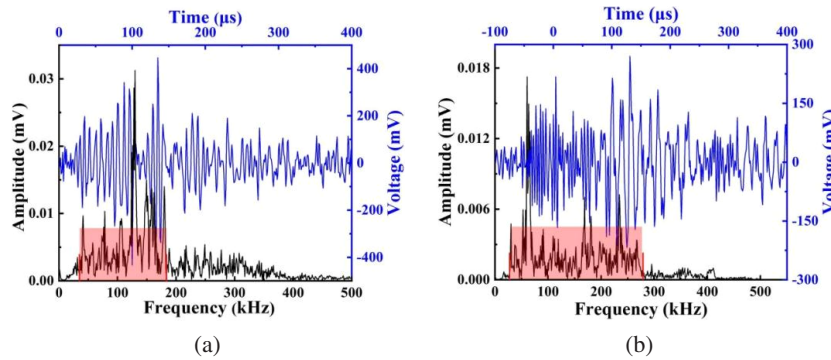

Fig. 9.   The time–domain curve of lead breaking waveform and the frequency–domain curve after FFT analysis of the sensor: (a) sensor A, (b) sensor B.

improving the bandwidth of the sensors through reducing the acoustic coupling interference.[1,30] The acoustic impedance of porous Al_2O_3 is 0.69 Mrayls, which is larger than that of air, resulting in a small acoustic reflection coefficient, as mentioned in Fig. 3 and Table 1. Moreover, the thermal and viscous effects in the pores make porous Al_2O_3 materials have the function of sound absorption.[31–34] As a result, these are useful to enhance acoustic attenuation property in the porous Al_2O_3. While for using air as the backing layer, the reverse is the case. Therefore, compared with air backing material, the sensor with porous Al_2O_3 can possess a wide bandwidth and low sensitivity.

Figure 10 presents the detection sensitivity of the sensor, which maintains a relatively stable state within the temperature range 25–500°C, but the amplitude of received signals shows a slightly decreasing tendency as the sensor temperature rising. Furthermore, the decrease of signal amplitude may be caused by the differences of thermal expansion of each component of the sensing system.[35] For instance, the difference of the thermal expansion coefficients of the sensor, steel ruler and conductive silver adhesive may increase the
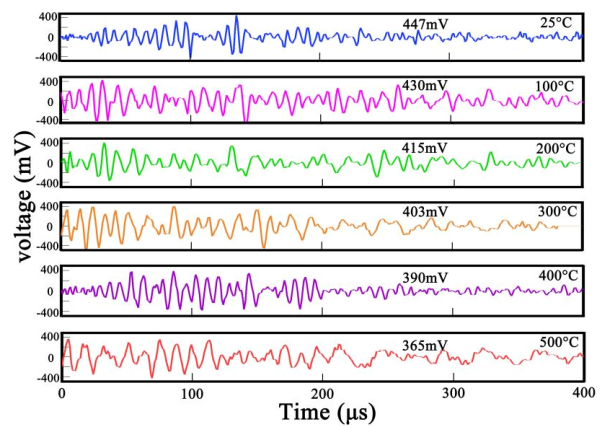

Fig. 10.   Variation of signal amplitudes of sensor A in the range 25–500°C.

impedance of AE signal propagation, resulting in the poorer acoustic coupling effect, and thus weakening the amplitude of the signal received by the system. Moreover, at the measuring temperature of 500°C, the signal amplitude can still
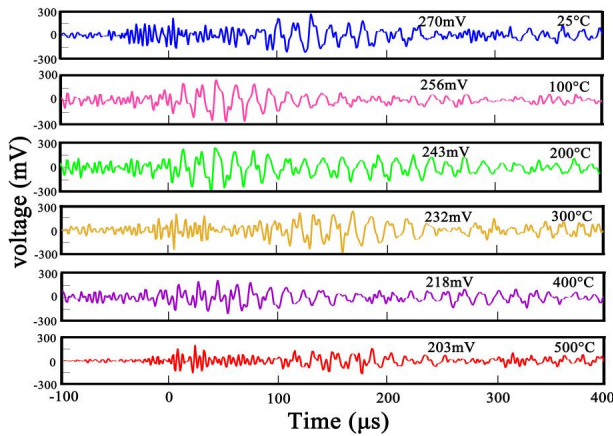
Fig. 11. Change of signal amplitudes of sensor B in the range 25–500°C.

reach 365 mV. In the wide temperature range 25– 500°C, the change rate of the maximum signal amplitude received by the sensor is only 18%, which indicates that the sensor can work stably in the high-temperature environment of 500°C.

As presented in Fig. 11, the waveform amplitude of sensor B has no significant change in trend from 25°C to 500°C. With the temperature increasing, the amplitude of received signal also decreases gradually, just as the change of sensor A. Within the range 25–500°C, the maximum signal amplitude decays from 270 mV to 203 mV, and then the change rate of the maximum signal amplitude can be calculated to be 25%. This result indicates that sensor B also has the capacity to work stably in a working temperature range 25–500°C.

4. Conclusions

In this work, using LGS crystals, two kinds of high-temperature AE sensors were designed and prepared with different backing layers. For sensor with air as the backing layer, the amplitude signal stimulated by the falling ball can reach 96 dB at 500°C, which is attenuated only about 3%. Also, the amplitude signal of sensor with porous Al_2O_3 backing layer has almost no attenuation in the temperature range 25–500°C. The variation ranges of the signal amplitudes are 447–365 mV and 270–203 mV at 25–500°C for the sensors with air and Al_2O_3 backing layers, respectively. Although the signal amplitude of sensor with Al_2O_3 backing is smaller, its bandwidth can be broadened to be 28–273 kHz, compared with 37–183 kHz for sensor with air backing. Based on the above results, these two kinds of sensors have stable and good ability at high-temperature of 500°C.

References

[1] W. K. Zhang, H. Y. Jia, G. P. Gao, X. Cheng, P. Du and D. Y. Xu, Backing layers on electroacoustic properties of the acoustic emission sensors, *Appl. Acoust.* **156**, 387 (2019).

[2] R. Guo, S. F. Huang and F. Liu, Study on preparation and simple calibration system of acoustic emission sensor based on epoxy resin, *J. Mater. Sci. Mater. Electron.* **33**(6), 3348 (2022).

[3] P. Wei, X. L. Han, D. Xia, T. L. Liu and H. Lang, Novel fiber-optic ring acoustic emission sensor, *Sensors* **18**(1), 215 (2018).

[4] F. Liu , R. Guo, X. J. Lin, X. F. Zhang, S. F. Huang, F. Yang and X. Cheng, Influence of propagation distance on characteristic parameters of acoustic emission signals in concrete materials based on low-frequency sensor, *Adv. Civ. Eng.* **2022**, 7241535 (2022).

[5] E. Tsangouri and D. G. Aggelis, A review of acoustic emission as indicator of reinforcement effectiveness in concrete and cementitious composites, *Constr. Build. Mater.* **224**, 198 (2019).

[6] I. D. Luch, M. Ferrario, D. Fumagalli, M. Carboni and M. Martinelli, Coherent fiber-optic sensor for ultra-acoustic crack emissions, *Sensors* **21**(14), 4674 (2021).

[7] G. L. Wang, L. F. Xie, C. Jiang, X. L. Liu, Y. L. Li, F. P. Yu and X. Zhao, High performance piezoelectric crystal cut designed using LiNbO3 for high temperature acoustic emission sensing application, *CrystEngComm* **24**(3), 691 (2021).

[8] A. Mohimi, T. Gan and W. Balachandran, Development of high temperature ultrasonic guided wave transducer for continuous in service monitoring of steam lines using non-stoichiometric lithium niobate piezoelectric ceramic, *Sens. Actuators A: Phys.* **216**, 432 (2014).

[9] Y. L. Du, G. R. Feng, H. P. Kang, Y. J. Zhang and X. H. Zhang, Effects of different pull-out loading rates on mechanical behaviors and acoustic emission responses of fully grouted bolts, *J. Cent. South Univ.* **28**(7), 2052 (2021).

[10] G. S. Su, W. Gan, S. B. Zhai and G. F. Zhao, Acoustic emission precursors of static and dynamic instability for coarse-grained hard rock, *J. Cent. South Univ.* **27**(10), 2883 (2020).

[11] C. Feng, Y. Y. Feng, M. J. Fan, C. H. Geng, X. J. Lin, C. H. Yang and S. F. Huang, $BiScO_3$-$BiFeO_3$-$PbTiO_3$-$BaTiO_3$ high-temperature piezoelectric ceramic and its application on high-temperature acoustic emission sensor, *J. Cent. South Univ.* **28**(12), 3747 (2021).

[12] X. L. Liu, G. D. Wang, M. Y. Li, J. G. Chen, S. X. Dong and Z. Q. Hu, Development of hard high-temperature piezoelectric ceramics for actuator applications, *J. Mater. Sci. Mater. Electron.* **26**(12), 9350 (2015).

[13] C. Han, C. Li, Y. L. Zhao, B. Li and X. Y. Wei, Research on a micro-processing technology for fabricating complex structures in single-crystal quartz, *Micromachines* **11**(3), 337 (2020).

[14] X. N. Jiang, K. Kim, S. J. Zhang, J. Johnson and G. Salazar, High-temperature piezoelectric sensing, *Sensors* **14**(1), 144 (2014).

[15] M. Schulz, J. Sauerwald, D. Richter and H. Fritze, Electromechanical properties and defect chemistry of high-temperature piezoelectric materials, *Ionics* **15**, 157 (2009).

[16] A. V. Sotnikov, H. Schmidt, M. Weihnacht, E. P. Smirnova, T. Y. Chemekova and Y. N. Makarov, Elastic and piezoelectric properties of AlN and $LiAlO_2$ single crystals, *IEEE Trans. Ultrason. Ferroelectr. Freq. Control* **57**(4), 808 (2010).

[17] C. L. Fei, X. L. Liu, B. P. Zhu, D. Li, X. F. Yang, Y. T. Yang and Q. F. Zhou, AlN piezoelectric thin films for energy harvesting and acoustic devices, *Nano Energy* **51**, 146 (2018).

[18]Z. A. A. R. Almaghbash, O. Arbouche, A. Dahani, A. Cherif, M. Belabbas and B. Djelloul, Signifcant improvement in the piezoelectric properties and electromechanical coupling factors of wurtzite AlN compound under high pressures, *J. Comput. Electron.* **20**(6), 2420 (2021).

[19]C. M. Lin, T. T. Yen, V. V. Felmetsger, M. A. Hopcroft, J. H. Kuypers and A. P. Pisano, Thermally compensated aluminum nit- ride Lamb wave resonators for high temperature applications, *Appl. Phys. Lett.* **97**, 083501 (2010).

[20]R. Fachberger, G. Bruckner, G. Knoll, R. Hauser, J. Biniasch and L. Reindl, Applicability of $LiNbO_3$, Langasite and $GaPO_4$ in high temperature SAW sensors operating at radio frequencies, *IEEE Trans. Ultrason. Ferroelectr. Freq. Control* **51**(11), 1427 (2004).

[21]K. Kim, S. J. Zhang, G. Salazar and X. N. Jiang, Design, fabrication and characterization of high temperature piezoelectric vibration sensor using YCOB crystals, *Sens. Actuators A: Phys.* **178**, 40 (2012).

[22]J. A. Johnson, K. Kim, S. J. Zhang, D. Wu and X. N. Jiang, High-temperature acoustic emission sensing tests using a yttrium calcium oxyborate sensor, *IEEE Trans. Ultrason. Ferroelectr. Freq. Control* **61**(5) 805 (2014).

[23]J. Bohm, R. B. Heimann, M. Hengst, R. Roewer and J. Schindler, Czochralski growth and characterization of piezoelectric single crystals with langasite structure: $La_3Ga_5SiO_{14}$ (LGS), $La_3Ga_{5.5}Nb_{0.5}O_{14}$ (LGN), and $La_3Ga_{5.5}Ta_{0.5}O_{14}$ (LGT), *J. Cryst. Growth* **204**, 128 (1999).

[24]T. Kim, J. Kim and X. N. Jiang, AlN ultrasound sensor for photoacoustic Lamb wave detection in a high temperature environment, *IEEE Trans. Ultrason. Ferroelectr. Freq. Control* **65**(8), 1444 (2018).

[25]J. Sauerwald, D. Richter, E. Ansorge, B. Schmidt and H. Fritze, Langasite based miniaturized functional structures: Preparation, high-temperature properties and applications, *Phys. Status Solidi A* **208**(2), 390 (2011).

[26]M. I. Shah and T. Saha, Optimal design of TSM langasite resonator for high-temperature applications: A review, *IEEE Trans. Ultrason. Ferroelectr. Freq. Control* **66**(5), 1465 (2021).

[27]C. Wong, S. Chan, W. C. Wu, C. Suen, H. Yau, D. Y. Wang, S. Li and J. Y. Dai, Tunable high acoustic impedance alumina epoxy composite matching for high frequency ultrasound transducer, *Ultrasonics* **116**, 106506 (2021).

[28]X. F. Zhang, X. J. Lin, R. Guo, C. H. Yang, H. Zhao, M. Y. Zhang, Y. Wang, X. Cheng and S. F. Huang, Influence of the prestressed layer on spherical transducer in sound radiation performance, *J. Adv. Dielect.* **12**(6), 2241004 (2022).

[29]K. Jemielniak, Some aspects of acoustic emission signal pre-processing, *J. Mater. Process. Tech.* **109**(3), 242 (2001).

[30]F. Liu, R. Guo, X. J. Lin, X. F. Zhang, S. F. Huang, F. Yang, X. Cheng, Monitoring the damage evolution of reinforced concrete during tunnel boring machine hoisting by acoustic emission, *Constr. Build. Mater.* **327**, 127000 (2022).

[31]L. T. Cao, Q. X. Fu, Q. Y. Si, B. Ding and J. Y. Yu, Porous materials for sound absorption, *Compos. Commun.* **10**, 25 (2018).

[32]U. Berardi and G. Iannace, Acoustic characterization of natural fibers for sound absorption applications, *Build. Environ.* **94**, 840 (2015).

[33]M. J. Cops, J. G. McDaniel, E. A. Magliula and D. J. Bamford, Analysis of thermal and viscous boundary layers in acoustic absorption by metallic foam, *J. Acoust. Soc. Am.* **146**(1), 649 (2019).

[34]P. Cobo and F. Simón, Multiple-layer microperforated panels as sound absorbers in buildings: A review, *Buildings* **9**(2), 53 (2019).

[35]R. Kazys and V. Vaskeliene, High temperature ultrasonic transducers: A review, *Sensors* **21**(9), 3200 (2021).